A Nested Spectral Model for Hurricane Track Forecasting

MARK DEMARIA, SIM D. ABERSON, AND KATSUYUKI V. OOYAMA

Hurricane Research Division, NOAA/AOML, Miami, Florida

STEPHEN J. LORD

National Meteorological Center, NOAA/NWS, Washington, D.C.

(Manuscript received 3 July 1991, in final form 25 November 1991)

ABSTRACT

A numerical method for analyzing and forecasting a wide range of horizontal scales of motion is tested in a barotropic hurricane track forecast model. The numerical method uses cubic B-spline representations of variables on nested domains. The spline representation is used for the objective analysis of observations and the solution of the prediction equations (shallow-water equations on a Mercator projection). This analysis and forecasting system is referred to as VICBAR (Vic Ooyama barotropic model).

The VICBAR model was tested in near real time during the 1989 and 1990 Atlantic hurricane seasons. For the 1989 season, VICBAR had skill comparable to, or greater than, that of the operational track forecast models. For the 1990 season, VICBAR had skill comparable to that of the operational track-forecast models. During both 1989 and 1990, VICBAR had considerably more skill for forecasts of hurricanes than for forecasts of tropical storms.

For the 1990 season, VICBAR was generalized to include time-dependent boundary conditions from a global forecast model. These boundary conditions improve the longer-range forecasts (60–72 h). The skill of VICBAR is sensitive to the choice of the background field used in the objective analysis and the fields used to apply the boundary conditions. The use of background fields and boundary-condition fields from a 12-h-old global model forecast significantly reduces the VICBAR skill (versus the use of fields from the current global forecast).

1. Introduction

Tropical cyclone circulations typically extend >1000 km outward from the storm center (e.g., Frank 1977) and can interact with synoptic-scale weather systems, such as midlatitude troughs and upper-level cold lows. However, the intense part of a tropical cyclone has a much smaller horizontal scale. The radius of low-level gale-force winds (17 m s^{-1}) is usually <400 km (Merrill 1984), and the radius of maximum wind can contract to less than 20 km in a strong hurricane (Willoughby et al. 1982). Therefore, a wide range of horizontal scales should be included when modeling tropical cyclones.

A numerical method based upon the spectral application of finite-element representation (SAFER method) has been developed (Ooyama 1984, 1987) to enable the inclusion of a range of horizontal scales in numerical models. The SAFER method represents dependent variables by truncated series of cubic beta splines (B splines), and was developed after consideration of a number of numerical requirements. A spectral method was chosen over a finite-difference method due to accuracy considerations. High-order finite-difference methods are available, but are difficult to implement in a domain with multiple-nested meshes. The requirement for flexible lateral boundary conditions eliminated the possibility of using spherical harmonics or Fourier components as a basis for the spectral method. General boundary conditions can be included when Chebyshev polynomials are used as a basis (Fulton and Schubert 1987); however, in that case, the resolution is concentrated near the boundaries of the domain. Given these restrictions, a finite-element representation was used. A desirable property for meteorological problems is differentiability up to second order. The cubic B splines were chosen to satisfy this requirement. Further details on the justification of the SAFER method can be found in Ooyama (1984).

As an application of the SAFER method, an analysis system and a barotropic hurricane track forecast model were developed. Observations are analyzed using a minimization algorithm in conjunction with B-spline representation of the analyzed fields. The forecast model uses the shallow-water equations to predict the B-spline amplitudes on a domain with nested meshes. This analysis and prediction system (referred to as VICBAR) was tested in near real time during the 1989

Corresponding author address: Dr. Mark DeMaria, NOAA/Hurricane Research Division, AOML, 4301 Rickenbacker Causeway, Miami, FL 33149.

and 1990 Atlantic hurricane seasons. The basic properties of the spline transforms are reviewed in section 2. In section 3, the design of the VICBAR model is described, and, in section 4, the results of near real-time track forecasts from the 1989 and 1990 hurricane seasons are presented.

2. Spline transforms

The basic properties of B-spline transforms were presented by Ooyama (1987) and Lord and Franklin (1987) in the context of the objective analysis of observations and by Ooyama (1984) in the context of a prediction model. The relevant properties of the SAFER method for analysis and prediction are summarized in this section. For simplicity, only one spatial dimension is considered. The results presented here can be generalized to two (horizontal) spatial dimensions.

Consider a function $\bar{u}(x)$ on the closed domain

$$x \in [x_0, x_N]. \tag{2.1}$$

The spline approximation to $\bar{u}$ is given by

$$u = \sum_{n=-1}^{N+1} a_n \phi_n(x), \tag{2.2}$$

where the basis functions ϕ_n are cubic B splines and a_n are the spline amplitudes. The ϕ_n are defined on a set of nodal points given by

$$x_n = x_0 + n\Delta x \quad n = -1, 0, \cdots, N+1, \tag{2.3}$$

where Δx is the nodal spacing. Each spline is a piecewise cubic polynomial where the function and its first and second derivatives are continuous at the nodal points. In the normalized coordinate ξ, the B spline Φ is defined by

$$\Phi(\xi) = \begin{cases} 0 & |\xi| \geq 2 \\ \frac{1}{4}(2 - |\xi|)^3 & 2 > |\xi| \geq 1 \\ \frac{1}{4}(2 - |\xi|)^3 - (1 - |\xi|)^3 & 1 > |\xi| \end{cases}, \tag{2.4}$$

where

$$\xi = \frac{x - x_n}{\Delta x}. \tag{2.5}$$

Figure 1 shows $\Phi(\xi)$ and its first three derivatives. Note that $\Phi(\xi)$ is symmetric about x_n and is nonzero over two nodal intervals on either side of x_n, and that the third derivative of Φ is piecewise continuous. The terms ϕ_{-1} and ϕ_{N+1} are included in the expansion (2.2), since they are nonzero over part of the domain defined by (2.1).

For homogeneous boundary conditions of the form

$$c_0 u + c_1 \frac{\partial u}{\partial x} + c_2 \frac{\partial^2 u}{\partial x^2} = 0 \quad \text{at} \quad x = x_0, x_N, \tag{2.6}$$

where c_0, c_1, and c_2 are constants, the spline amplitudes a_{-1} and a_{N+1} can be calculated from the remaining spline amplitudes using

$$\left.\begin{aligned} a_{-1} &= \frac{a_0[-c_0 + (3c_2/\Delta x^2)] - a_1[(c_0/4) + (3c_1/4\Delta x) + (3c_2/2\Delta x^2)]}{(c_0/4) - (3c_1/4\Delta x) + (3c_2/2\Delta x^2)} \\ a_{N+1} &= \frac{a_N[-c_0 + (3c_2/\Delta x^2)] - a_{N-1}[(c_0/4) - (3c_1/4\Delta x) + (3c_2/2\Delta x^2)]}{(c_0/4) + (3c_1/4\Delta x) + (3c_2/2\Delta x^2)} \end{aligned}\right\}. \tag{2.7}$$

Equations (2.7) are derived by substitution of (2.2) into (2.6), using (2.4)–(2.5) to determined ϕ_n and its derivatives, evaluating the series from (2.2) at x_0 or x_N, and then solving (2.6) for a_{-1} or a_{N+1}.

The remaining spline amplitudes are determined from a standard least-squares approximation. Let the norm of a function $f(x)$ be defined as

$$\|f(x)\| = (f, f)^{1/2}, \tag{2.8}$$

where the parentheses denote the inner product given by

$$(f, g) = \int_{x_0}^{x_N} (fg)dx. \tag{2.9}$$

The error E between the function $\bar{u}$ and its spline approximation u is then given by

$$E = \|u - \bar{u}\|. \tag{2.10}$$

For the least-squares fit, the spline amplitudes a_n for $n = 0, 1, \cdots, N$ are chosen so that E is minimized. Using (2.2) to eliminate u in (2.10) and setting $\partial E/\partial a_n = 0$ for $n = 0, 1, 2, \cdots, N$ to find the minimum of E gives

$$\sum_{n'=-1}^{N+1} a_{n'}(\phi_{n'}, \phi_n) = (\bar{u}, \phi_n), \quad n = 0, 1, \cdots, N. \tag{2.11}$$

If (2.7) is used to eliminate a_{-1} and a_{N+1}, then (2.11) can be written as

$$\mathbf{Pa} = \mathbf{b}, \tag{2.12}$$

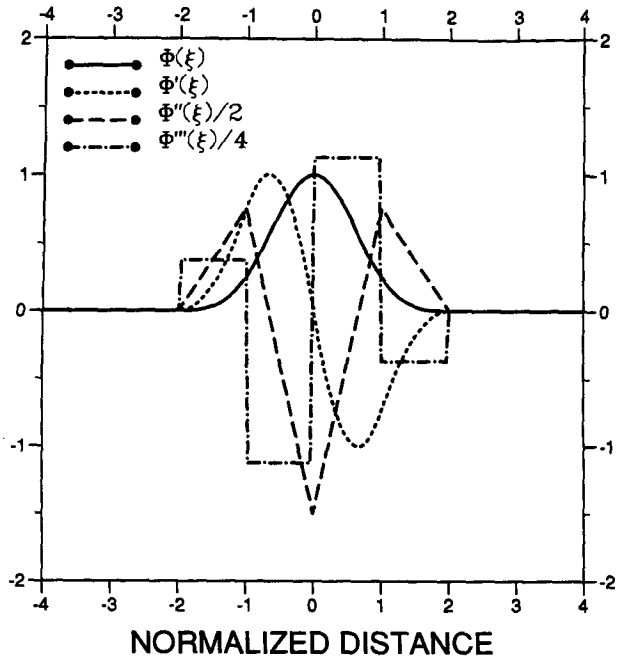

FIG. 1. The cubic-spline function $\Phi(\xi)$ and its first three derivatives in normalized coordinates $\xi = (x - x_n)/\Delta x$.

where

$$\left.\begin{aligned}\mathbf{a} &= (a_0, a_1, \cdots, a_N)^{\mathrm{T}} \\ \mathbf{b} &= (b_0, b_1, \cdots, b_N)^{\mathrm{T}}\end{aligned}\right\} \tag{2.13}$$

$$b_n = (\bar{u}, \phi_n), \tag{2.14}$$

and $\mathbf{P}$ is an $N + 1 \times N + 1$ matrix whose elements contain linear combinations of $(\phi_{n'}, \phi_n)$. Because $\phi_n(x)$ is zero outside of the interval $(x_n + 2\Delta x, x_n - 2\Delta x)$, the matrix $\mathbf{P}$ is banded with three nonzero elements on each side of the diagonal.

The procedure for determining the spline amplitudes requires the evaluation of the integrals in (2.14) and in the elements of $\mathbf{P}$. If $\bar{u}$ is a polynomial, then these integrals can be determined analytically. In practice, Gaussian quadrature is used for the integration, with two quadrature points per nodal interval. The elements of $\mathbf{P}$ need only be determined once for a given mesh configuration. The spline approximation to the function $\bar{u}$ is then determined in three steps. First, the function $\bar{u}$ is evaluated at the Gaussian quadrature points. Next, the elements of $\mathbf{b}$ are determined from (2.14). The banded linear system (2.12) is then solved for the spline amplitudes $\mathbf{a}$, where (2.7) is used to determine a_{-1} and a_N.

As an example of the use of the spline transforms to solve differential equations, consider the nonlinear advection equation with homogeneous boundary conditions given by

$$\frac{\partial u}{\partial t} + u\frac{\partial u}{\partial x} = 0, \tag{2.15}$$

$$u(x_0, t) = u(x_N, t) = 0, \tag{2.16}$$

and

$$u(x, 0) = \bar{u}(x). \tag{2.17}$$

Now, assume $u(x, t)$ is expanded in a series of the form (2.2) where the amplitudes a_n are functions of time. For the boundary conditions in (2.16), a_{-1} and a_{N+1} are given by (2.7) with $c_1 = c_2 = 0$ and $c_0 = 1$. The initial spline amplitudes are determined by evaluating $\bar{u}(x)$ at the Gaussian grid points, calculating $\mathbf{b}$ using (2.14), and solving (2.12) for $\mathbf{a}$. To integrate $u(x, t)$ forward in time, take the inner product of (2.15) with ϕ_n, which gives

$$\frac{\partial b_n}{\partial t} = -\left(u\frac{\partial u}{\partial x}, \phi_n\right). \tag{2.18}$$

Since the initial amplitudes $\mathbf{a}$ have been calculated, u and $\partial u/\partial x$ can be evaluated at the Gaussian grid points ($\partial u/\partial x$ is found by differentiating the spline expansion and evaluating the result on the grid points). Then the inner product on the right side of (2.18) is evaluated using Gaussian quadrature and b_n is integrated in time using a finite-difference approximation to $\partial b_n/\partial t$. In general, centered time differences (with an initial forward step) are used for advective terms and forward time differences are used for diffusion and friction terms. Once b_n is determined at the next time step, $\mathbf{a}$ can be updated using (2.12) and (2.7) and the process can be repeated.

When nested meshes are used, the time-stepping procedure becomes slightly more complicated. Consider the mesh structure shown in Fig. 2, where upper- (lower-) case symbols denote the coarse (fine) mesh. The spline expansions on the two meshes are given by

$$u(x, t) = \sum_{n=-1}^{N+1} a_n(t)\phi_n(x) \quad \text{(fine mesh)} \tag{2.19}$$

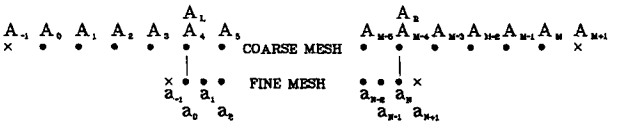

FIG. 2. The nested-mesh structure for the case in which the nodal spacing increases by a factor of 2 from the fine to the coarse mesh. The fine-mesh domain extends from node 4 to node $M - 4$ on the coarse mesh. The coarse-mesh amplitudes at the left and right interfaces with the fine mesh are denoted A_L and A_R. The dots and crosses denote nodal points inside and outside of the model domain, respectively.

and

$$u(x, t) = \sum_{m=-1}^{M+1} A_m(t)\Phi_m(x) \quad \text{(coarse mesh)}. \quad (2.20)$$

At the boundaries of the coarse mesh, assume that a homogeneous boundary condition is applied so that A_{-1} and A_{M+1} are determined from (2.7). The remaining A_m can be evaluated from equations that are analogous to (2.12)–(2.14). At the left interface u, $\partial u/\partial x$, and $\partial^2 u/\partial x^2$ are assumed continuous, which gives

$$\begin{pmatrix} a_{-1} \\ a_0 \\ a_1 \end{pmatrix} = \begin{pmatrix} 1/2 & 1/2 & 0 \\ 1/8 & 3/4 & 1/8 \\ 0 & 1/2 & 1/2 \end{pmatrix} \begin{pmatrix} A_{L-1} \\ A_L \\ A_{L+1} \end{pmatrix}, \quad (2.21)$$

where A_L is the coarse-mesh amplitude at the node of the mesh interface on the left side of the fine mesh. A similar condition can be derived for the interface at the right side of the fine mesh. Thus, on the fine mesh a_{-1}, a_0, a_1 and a_{N-1}, a_N, a_{N+1} are determined from the coarse-mesh amplitudes. The remaining fine-mesh amplitudes are determined from the least-squares constraint.

For efficiency of the model, a larger time step on the coarse mesh should be used. For a coarse–fine-mesh ratio of 2:1, a time step of $2\Delta t$ can be used on the coarse mesh where Δt represents the fine-mesh time step. For this case, the time integration of the nonlinear advection equation would proceed as follows, where lower- (upper-) case symbols refer to the fine (coarse) meshes and $\mathbf{P}_f$ and $\mathbf{P}_c$ represent the coefficient matrices that result from the least-squares condition on the fine and coarse meshes.

1) Determine $\mathbf{b}$ at $t = 0$ using $b_n = (\bar{u}, \phi_n)$.
2) Determine $\mathbf{B}$ at $t = 0$ using $B_m = (\bar{u}, \Phi_m)$.
3) Determine $\mathbf{A}$ at $t = 0$ using $\mathbf{P}_c\mathbf{A} = \mathbf{B}$ and homogeneous boundary conditions.
4) Determine $\mathbf{a}$ at $t = 0$ using $\mathbf{P}_f\mathbf{a} = \mathbf{b}$ and the interface conditions.
5) Determine $\mathbf{B}$ at $t = 2\Delta t$ using time differencing.
6) Determine $\mathbf{A}$ at $t = 2\Delta t$ using $\mathbf{P}_c\mathbf{A} = \mathbf{B}$ and homogeneous boundary conditions.
7) Determine $\mathbf{b}$ at $t = \Delta t$ using time differencing.
8) Determine $\mathbf{a}$ at $t = \Delta t$ using $\mathbf{P}_f\mathbf{a} = \mathbf{b}$ and the interface conditions.
9) Determine $\mathbf{b}$ at $t = 2\Delta t$ using time differencing.
10) Determine $\mathbf{a}$ at $t = 2\Delta t$ using $\mathbf{P}_f\mathbf{a} = \mathbf{b}$ and the interface conditions.
11) Repeat steps 5–10 for the next coarse-mesh time step.

In step 8, the coarse-mesh amplitudes at $t = \Delta t$ are required for the interface conditions. Since the time step on the coarse mesh is $2\Delta t$, the required amplitudes are linearly interpolated in time using the coarse-mesh amplitudes at $t = 0$ and $t = 2\Delta t$. The interface conditions provide the feedback from the coarse to the fine mesh.

The updated values of B_m are determined by integrating

$$\frac{\partial B_m}{\partial t} = -\left(u\frac{\partial u}{\partial x}, \Phi_m\right) \quad (2.22)$$

in time. When the right side of (2.22) is evaluated, the coarse-mesh representation of $u(x, t)$ given by (2.20), is used to evaluate u and $\partial u/\partial x$ on the domain outside of the fine-mesh region. On the part of the domain covered by both the fine and coarse meshes, the fine-mesh representation of $u(x, t)$ given by (2.19) is used to evaluate the right side of (2.22). The use of the fine-mesh representation of $u(x, t)$ to evaluate the right side of (2.22) provides the feedback from the fine to the coarse mesh.

When elliptic equations are solved, the coarse-mesh region must cover the entire fine-mesh domain, because forcing in the interior of the domain affects the solution over the entire domain. However, when hyperbolic equations are solved, the coarse and fine meshes must overlap, but the overlap should be kept to a minimum. Small spatial oscillations near the mesh interface that result from representing the fine-mesh information on the coarse mesh accumulate during time integrations if the coarse mesh extends too far into the fine-mesh region. In the numerical solution of shallow-water equations described later, the coarse mesh extends one coarse-mesh nodal spacing into the fine-mesh domain.

When information is transferred from the fine to the coarse mesh, or when splines are fitted to observations, we find that it is useful to include a spatial filter in the spline transformation. This inclusion is accomplished by adding a penalty term E_p to the error E, defined by (2.10), so that the total error E_t is given by

$$E_t = (E^2 + E_p^2)^{1/2}, \quad (2.23)$$

where

$$E_p = \left\| a^{1/2}\frac{d^k u}{dx^k} \right\|, \quad k = 1, 2, \text{ or } 3. \quad (2.24)$$

The term E_p constrains the derivative of the spline expansion, and the parameter a (which can be a function of x) controls the strength of the constraint.

To illustrate the effect of the constraint term in (2.23), consider the case where u is a general function of x (not a truncated B-spline series) and a is a constant. The Euler–Lagrange equation that corresponds to the functional (2.23) is given by

$$(-1)^k a\frac{d^{2k}u}{dx^{2k}} + u = \bar{u}. \quad (2.25)$$

That is, the function $u(x)$ that minimizes the functional

(2.23) is also the solution to the differential equation (2.25). Now consider the case where $x \in [0, L]$, $u(0) = u(L) = 0$, and $\bar{u} = A \sin 2\pi x/L$. Then the solution to (2.25) is given by

$$u = \left[\frac{1}{1 + (L_c/L)^{2k}}\right] A \sin \frac{2\pi x}{L}, \qquad (2.26)$$

where

$$L_c = 2\pi a^{1/(2k)}. \qquad (2.27)$$

Equation (2.26) shows that when the forcing is a sine wave, the response is also a sine wave, but with a reduced amplitude. The shape of the response function is determined by the order of the derivative k in (2.24). The half-amplitude wavelength of the response function is given by L_c. Thus, the derivative constraint term in (2.23) acts as a low-pass spatial filter that can be adapted to a particular problem by careful choices of a and k. In the objective analyses, a is constant on each mesh, and in the solution of the shallow-water equations, a increases toward the edge of each mesh and is continuous across each mesh interface. The spatial variation of a is used to gradually filter the fine-mesh information as it approaches the coarse mesh in the solution of the prediction equations.

For the case with constant a, the choice of spline amplitudes to minimize E_t leads to a linear system of the form

$$(\mathbf{P} + a\mathbf{Q})\mathbf{a} = \mathbf{b}, \qquad (2.28)$$

where $\mathbf{Q}$ is a matrix with a banded structure similar to $\mathbf{P}$. The elements of $\mathbf{Q}$ contain linear combinations of inner products of the derivatives of the basis functions ϕ_n. When a is a function of x, $\mathbf{Q}$ has the same banded structure as before, but a cannot be factored out of the integrals that are required to calculate the elements of $\mathbf{Q}$.

The definition of the error (2.23) is appropriate for the case when functions of x are fitted with splines. The splines can also be used to objectively analyze observations. Consider the case where J observations $\bar{u}_j$ are located at points x_j in the domain defined by (2.1). To fit the spline expansion (2.2) to this field of observations, the total error E_t in (2.23) is modified by replacing E with a discrete form of the error (E_d) so that

$$E_t' = (E_d^2 + E_p^2)^{1/2}, \qquad (2.29)$$

where

$$E_d^2 = \sum_{j=1}^{J} w_j (u_j - \bar{u}_j)^2 \Delta x, \qquad (2.30)$$

u_j is the spline expansion evaluated at the observation point x_j, and w_j is an arbitrary data weight.

Setting the derivative of E_t' with respect to a_n to zero in (2.29) (for the case with constant a) leads to a linear system of the form

$$(\mathbf{P}' + a\mathbf{Q})\mathbf{a} = \mathbf{b}', \qquad (2.31)$$

where the elements of $\mathbf{P}'$ contain linear combinations of

$$\sum_{j=1}^{J} w_j \Big[\sum_{n'=-1}^{N+1} \phi_{n'}(x_j)\phi_n(x_j) \Big] \qquad (2.32)$$

and $\mathbf{b}'$ is a vector with elements defined by

$$b_n' = \sum_{j=1}^{J} w_j \bar{u}_j \phi_n(x_j) \Delta x. \qquad (2.33)$$

The matrix $\mathbf{P}'$ has a banded structure similar to $\mathbf{P}$, and $\mathbf{Q}$ in (2.31) is identical to that in (2.28). When the observations $\bar{u}_j$ are sparse, some additional elements of $\mathbf{P}'$ may be zero relative to corresponding elements of $\mathbf{P}$. However, because $\mathbf{Q}$ is derived from the E_p term, which is in continuous form in (2.29), $\mathbf{P}' + a\mathbf{Q}$ is nonsingular and (2.31) can be solved for $\mathbf{a}$.

When the splines are fitted to observations, the values of a and k in the E_p term should be chosen on the basis of the observation distribution. The weights w_j in (2.30) can be assigned on the basis of observation type. A direct measurement of a quantity (for example, from a rawinsonde) might be assigned a higher weight than an indirect measurement of a quantity (for example, from a satellite). The weights can also be used to compensate for the variation in the density of different types of observations. A density weighting scheme has been developed where the weight is the ratio of the total number of nodal cells in the domain that have at least one observation of a given type to the total number of observations of that type. In one dimension, a nodal cell is the part of the x domain between the nodal points defined by (2.3). In two dimensions, a nodal cell is the rectangular area between consecutive nodal points in x and y. In a nested analysis, the density-weighting scheme is first applied on the interior mesh. For the next-larger mesh (coarse mesh), the weights on the interior mesh are divided by the ratio of the nodal cell area on the interior mesh to that on the coarse mesh. The weights for the observations on the part of the coarse mesh not covered by the interior mesh are determined by a separate application of the density-weighting scheme. This process is repeated on each larger mesh. This modification of the density-weighting scheme in the nested analysis is necessary for the case where there are numerous observations of a particular type near the center of a coarse mesh, but fewer observations in the region that does not overlap with the next interior mesh. Without this modification the weight of the observations away from the center of the mesh would be too low.

General software for solving systems of differential

equations using the spline transforms on arbitrary numbers of nested horizontal (x, y) meshes has been developed with an option for all but the outer mesh to move during time integrations. When nested domains are used for the analysis of observations, the coarse-mesh domain must cover the entire fine-mesh domain (similar to the case when elliptic equations are solved, as previously described). In the next section, the application of this general software to a barotropic hurricane track forecast model is described.

3. A barotropic hurricane track forecast model

As an application of the SAFER software, a barotropic hurricane track forecast model was developed. The forecasting system consists of an objective analysis system and a barotropic prediction model, both of which utilize the spline representation of variables on nested domains. This forecasting system is referred to as VICBAR (Vic Ooyama barotropic model).

The VICBAR model was developed and tested during the 1989 Atlantic hurricane season. For the 1990 season, a number of changes were made to the model. Based on the 1990 results, some additional changes were made in preparation for the 1991 season. The most general version of the model is described in this section. The modifications for each individual year will be described in section 4 when the forecast results are presented.

a. Prediction model

The prediction model is governed by the shallow-water equations on a Mercator projection, which can be written as

$$\frac{\partial u}{\partial t} + m\left(u\frac{\partial u}{\partial x} + v\frac{\partial u}{\partial y}\right) - \left(f + \frac{u\tan\theta}{a}\right)v + mg\frac{\partial h}{\partial x} = -\gamma(u - \bar{u}), \quad (3.1)$$

$$\frac{\partial v}{\partial t} + m\left(u\frac{\partial v}{\partial x} + v\frac{\partial v}{\partial y}\right) + \left(f + \frac{u\tan\theta}{a}\right)u + mg\frac{\partial h}{\partial y} = -\gamma(v - \bar{v}), \quad (3.2)$$

and

$$\frac{\partial h}{\partial t} + m\left(u\frac{\partial h}{\partial x} + v\frac{\partial h}{\partial y}\right) + m^2(H + h) \times \left[\frac{\partial}{\partial x}\left(\frac{u}{m}\right) + \frac{\partial}{\partial y}\left(\frac{v}{m}\right)\right] = -\gamma(h - \bar{h}), \quad (3.3)$$

where x and y are the distances east and north on the Mercator projection, u and v are horizontal velocity components, h is the deviation fluid depth, H is the mean fluid depth, $\bar{u}$, $\bar{v}$, $\bar{h}$ are specified functions, γ is a nudging coefficient, f is the Coriolis parameter ($2\Omega \times \sin\theta$, where θ is latitude and Ω is the earth's angular speed), g is the acceleration of gravity, a is the earth's radius, and m is the map factor defined by

$$m = \frac{\cos\theta_0}{\cos\theta}, \quad (3.4)$$

where θ_0 is the reference latitude.

In the foregoing equations, $H = 750$ m, $\Omega = 7.292 \times 10^{-5}$ s^{-1}, $g = 9.8$ m s^{-1}, $a = 6371$ km, and $\theta_0 = 30°$N. Some care was required in the determination of H. The mean fluid depth plays a role similar to the divergence correction in a balanced barotropic (vorticity equation) model (Leith 1974). In the balanced model, a term of the form $1/R^2$ is added to the Laplacian operator that relates the vorticity and streamfunction. The constant R can be interpreted as the Rossby radius of deformation c/f_0, where c is a gravity-wave speed $(gH)^{1/2}$ and f_0 is a reference value of the Coriolis parameter. This factor prevents the retrogression of long Rossby waves and leads to improved barotropic predictions (Cressman 1958). Leith (1974) has shown that 500-mb geopotential height errors in an ensemble of forecasts were minimized for $R \sim 800$ km and that the errors were not very sensitive to the choice of R provided that the value was less than $\sim$1300 km. At 30°N, $R \sim 1300$ km corresponds to $H \sim 900$ m and $R \sim 800$ km corresponds to $H \sim 350$ m. The value $H = 750$ m was chosen since this was the smallest value that would ensure that the total fluid depth was always positive on the model domain. A series of sensitivity experiments were performed with $H = 1500$ and 5000 m. These results were in agreement with Leith (1974) in that the track errors with $H = 1500$ m were nearly identical to those in the $H = 750$ m case, but slightly smaller than the errors in the $H = 5000$ m case.

Equations (3.1)–(3.3) are solved using the SAFER method on a sequence of nested meshes, where the spline nodal spacing and time step increase by a factor of 2 on each larger mesh. The inner meshes move to remain centered on the storm, and the outer domain is fixed geographically. The dependent variables and their first and second derivatives are continuous across each mesh interface, as described in section 2. For the outer domain, two types of lateral boundary conditions can be applied. When fields are available from another model (for example, from a global spectral model), the γ terms in (3.1) and (3.2) are used to impose the boundary conditions. For this case, $\bar{u}$, $\bar{v}$, and $\bar{h}$ are determined from the other model and γ is a specified function of x, y, and t that controls the rate at which the predicted fields are forced to the boundary values. The function γ was chosen so that the fields away from the storm would be primarily determined from $\bar{u}$, $\bar{v}$, and $\bar{h}$, while close to the storm the fields would be determined by the barotropic model. The function γ is given by

$$\gamma(r) = \begin{cases} 0 & r \leq r_I \\ \gamma_0/2\left\{1 - \cos\left[\left(\dfrac{r - r_I}{r_0 - r_I}\right)\pi\right]\right\} & r_I < r < r_0 \\ \gamma_0 & r_0 \leq r \end{cases}, \quad (3.5)$$

where r is the radius from the storm center and r_I, r_0, and γ_0 are constants. The function γ is time dependent, since the storm center moves during the time integration. The constants r_I, r_0, and γ_0 were chosen as 1500 km, 2500 km, and 10^{-4} s^{-1}, respectively. If $\bar{u}$ were constant with time and all the terms on the left side of (3.1) were neglected except the time tendency, $(u - \bar{u})$ would decay exponentially with an e-folding time of $1/\gamma_0$. For $\gamma_0 = 10^{-4}$ s^{-1}, the e-folding time is slightly <3 h, indicating that fields are primarily determined by the boundary conditions for $r > r_0$. For $r < r_I$, the forcing terms are zero and the fields are determined by the barotropic prediction. The area with $r_I < r < r_0$ is a transition region between the barotropic prediction and the boundary conditions (γ increases from 0 to γ_0 as r increases from r_I to r_0).

If fields from another model were not available, γ was set to zero and a different lateral boundary condition was applied. At the outer boundary of the largest mesh, the second derivatives of u, v, and h normal to the boundary were set to zero. With this boundary condition, the advective terms in (3.1)–(3.3) can cause uncontrolled growth in the prognostic variables near the edges of the domain. To overcome this problem, the amplitudes $A(t)$ on the outer domain were relaxed back to their initial values after each large-mesh time step using

$$A(t + \Delta t) = (1 - \epsilon)A^*(t + \Delta t) + \epsilon A(0), \quad (3.6)$$

where $A^*(t + \Delta t)$ is the spline amplitude predicted by the prognostic equations and ϵ is a factor between 0 and 1. If $\epsilon = 1$ everywhere on the largest mesh, u, v, and h will be constant in time. In practice, $\epsilon = 0.5$ on the largest-mesh boundary and decreases to zero at the interface with the next-largest mesh. A "loose" fit to the initial condition is preferable to a "tight" fit on the outer domain. With this boundary condition, it was necessary to fix the outer two meshes geographically.

The model is initialized with vertically averaged horizontal winds and geopotential heights. The winds on all of the meshes and the heights on the outer mesh are interpolated from the objective analysis. On the interior meshes, the initial heights are determined from the balance equation, which can be written as

$$m^2 g\nabla^2 h = \zeta f - \beta u - 2m^2\left(\frac{\partial v}{\partial x}\frac{\partial u}{\partial y} - \frac{\partial u}{\partial x}\frac{\partial v}{\partial y}\right) + \frac{\tan\theta}{a}u\zeta - \frac{m\tan\theta}{a} \times \left[u\left(\frac{\partial v}{\partial x} + \frac{\partial u}{\partial y}\right) - v\left(\frac{\partial u}{\partial x} - \frac{\partial v}{\partial y}\right)\right] - \frac{(u^2 + v^2)(1 + \tan^2\theta)}{a^2}, \quad (3.7)$$

where $\beta = df/dy$ and $\zeta = m(\partial v/\partial x - \partial u/\partial y) + u \times \tan\theta/a$. Equation (3.7) is determined by deriving the divergence equation from (3.1) and (3.2) and then setting the divergence and its time tendency to zero. The balance equation determines h on the interior meshes using the observed heights on the outer mesh as boundary conditions. The balance equation is solved using the SAFER method, where the coarse-mesh domains cover all of the fine-mesh domains. Once the time integration begins, the coarse-mesh domains for h (and u and v) overlap the fine-mesh domains by one coarse-mesh nodal interval.

b. *Objective analysis*

The barotropic prediction model requires vertically averaged winds and heights. These are obtained from analyses at several pressure levels between 200 and 850 mb. Information below 850 and above 200 mb was not included since these levels are influenced by boundary-layer processes and the storm outflow, respectively, and are not representative of the storm motion. The winds and heights at each pressure level were analyzed on three horizontal domains (synoptic-scale domain, storm-environment domain, and vortex domain).

The synoptic-scale domain covers a region slightly larger than the outer mesh of the prediction model (~150° span of longitude, ~80° span of latitude). On this domain, winds and heights on a 2.5° lat–long grid are obtained directly from either the NMC regional analysis (1989 VICBAR), a 12-h forecast from the National Meteorological Center (NMC) global model (1990 VICBAR), or from the initial condition for the NMC global model (1991 VICBAR).

The storm-environment domain covers a 30° lat–long area centered on the storm. On this domain, single-mesh spline analyses are performed at each pressure level using the NMC winds and heights on the 2.5° grid as a background field.[1] The spline analyses include rawinsonde data and satellite cloud-track winds obtained from the NMC operational data files and special aircraft observations when available. The aircraft data

[1] The term *background field* will be used to describe the gridded fields obtained from NMC, whether they are from an analysis (1989 and 1991 VICBAR) or a model forecast (1990 VICBAR). The term *first-guess field* is sometimes used, but strictly speaking, this applies to the starting point of an iterative procedure such as the method of successive corrections. Since the spline analysis is not an iterative method, the term *first-guess field* is avoided.

include observations from air force reconnaissance and NOAA research-reconnaissance missions that are transmitted to the National Hurricane Center (NHC) in real time. In the spline analyses, a third-order filter ($k = 3$) with a half-amplitude wavelength L_c of 4° latitude is used (see 2.26 and 2.27). All observations are given a relative weight w_j of 1.0, while the background field has a relative weight of 0.2 (see 2.30). The density-weighting scheme is applied to each observation type and the background field.

The spline analyses on the storm-environment domain include smaller-scale information than the analyses on the synoptic-scale domain. However, in most cases, the data coverage is inadequate to accurately represent the vortex circulation. For this reason, bogus wind observations are added on a third domain (vortex domain), which covers a circular area with a radius of 600 km, centered on the storm. These bogus observations are added in a cylindrical coordinate system with a radial grid spacing of 25 km and an azimuthal grid spacing of 22.5° (16 azimuthal points at each radius).

The winds on the vortex grid are the sum of an axisymmetric vortex and a constant vector. The constant vector represents the initial storm motion and is obtained from the forecasters at NHC. The axisymmetric vortex is given by

$$V = V_m\left(\frac{r}{r_m}\right)\exp\left\{\frac{1}{b}\left[1 - \left(\frac{r}{r_m}\right)^b\right]\right\}, \quad (3.8)$$

where V is the tangential wind, r is the radius, V_m is the maximum tangential wind, r_m is the radius of maximum wind, and b is a size parameter. The parameters V_m, r_m, and b are determined from storm information estimated by the NHC forecasters; V_m is set to 0.8 times the operational maximum wind estimate. The factor of 0.8 accounts for the bogus vortex representing the 850–200-mb vertically averaged tangential wind, which is typically less than the maximum low-level wind (e.g., Frank 1977). The relationships between operational storm information and the parameters r_m and b were determined from a set of 11 cases from 1982 to 1988 that had National Oceanic and Atmospheric Administration (NOAA) Omega dropwindsonde (ODW) data available in the outer portion of the storm and NOAA or U.S. Air Force data in the interior of the storm. The radius of maximum wind r_m is 1.1 times the operational eye-size estimate. The operational eye size is always specified by NHC, even for weak systems. Typically, the eye-size estimate is about 40 km for weak systems. The size parameter b is determined so that the 5 m s^{-1} tangential wind occurs at a specified radius r_5 given by

$$r_5 = 250 + r_I, \quad (3.9)$$

where r_I is the operational influence radius in kilometers. The influence radius is determined by the forecasters from surface analyses and satellite loops and represents the radius of the area influenced by the storm circulation. Figure 3 shows examples of the vortex profile used for Hurricane Dean (V_m = 29 m s^{-1}, r_m = 51 km, b = 0.393) and Hurricane Gabrielle (V_m = 47 m s^{-1}, r_m = 61 km, b = 0.414) from 1989. Dean was a small- to average-sized storm, and Gabrielle was a large storm.

The vertically averaged analysis on the synoptic-scale domain (2.5° grid), the vertically averaged spline analysis on the storm environment domain (evaluated on a 1° grid), and the bogus winds on the vortex domain (cylindrical grid) are blended through use of a nested version of the spline analysis. Several meshes are used with a mesh structure that is similar to that of the prediction model. For the nested analysis, we excluded the input from the synoptic-scale domain over a 24° lat–long area centered on the storm and the input from the storm-environment domain within 333 km of the storm. This modification allows the information from the synoptic-scale, storm-environment, and vortex domains to overlap, but prevents information from the synoptic-scale and storm-environment domains from being used near the storm center.

The winds and heights from the nested analysis are interpolated to the Gaussian grid point of the nested prediction model. The height analysis near the storm is inconsistent with the wind analysis because bogus heights are not included on the vortex domain and heights are unavailable at the locations of the satellite cloud-track winds in the storm-environment analysis. Therefore, the heights on the inner meshes are determined from the balance equation, as described previously.

Numerous studies (e.g., DeMaria 1985) have shown that the vortex structure within ~100 km of the storm

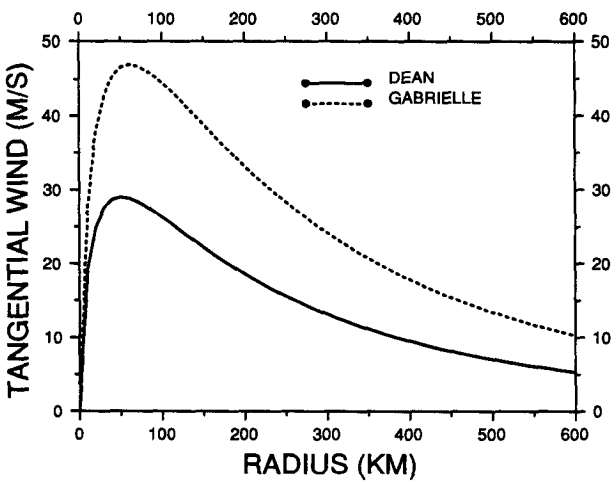

FIG. 3. Vortex profiles representing the vertically averaged tangential wind for Hurricane Dean at 0000 UTC 4 August 1989 and for Hurricane Gabrielle at 0000 UTC 7 September 1989.

center has very little influence on the vortex track in barotropic models. For this reason, a nodal spacing of 50 km was used on the inner mesh of the prediction model. A 4° latitude filter was applied to the inner mesh of the nested analysis to ensure that the resolution of the analysis was compatible with the model resolution. With this resolution, the single-mesh analyses on the storm-environment domain required about 5 min of CPU time on a VAX-8700, and the nested analysis and 72-h forecast required about 5 min of CPU time on a CYBER-205. Figure 4 shows an example of the initial wind and height field for Hurricane Dean on the inner three meshes of the prediction model after the balance equation has been applied. The inner part of the vortex has been smoothed by the 4° latitude filter on the inner mesh of the nested analysis.

To illustrate the lack of sensitivity of the predicted track to the inner structure of the vortex, the forecast for Dean at 0000 UTC 4 August 1989 was run with three additional interior meshes in the nested analysis and two additional interior meshes in the prediction model. In this case, the resolution near the vortex center is about 12 km (compared with 50-km resolution in the operational prediction model). Figure 5 shows the initial wind field near the vortex center for the operational and high-resolution versions of the model. The high-resolution model resolves the inner structure of the bogus vortex, as indicated by the greater maximum wind and smaller radius of maximum wind. Despite the increased resolution, the vortex positions in the operational and high-resolution forecasts differed by less than 30 km at all times between 0 and 72 h over a track length of about 1500 km. The difference in the forecast errors was less than 20 km at all times between 0 and 72 h, and the low-resolution model had a slightly smaller forecast error at 72 h. Several other cases were tested, and the results confirmed that there was no consistent decrease in the forecast errors with the high-resolution model.

Although the track of the vortex in the barotropic model is not sensitive to the inner structure of the vortex, it is sensitive to the outer structure (~400–800 km). The outer structure of the bogus vortex defined by (3.7) is primarily controlled by v_m and b. Because of this sensitivity, these parameters were determined from the available operational storm parameters, as described previously.

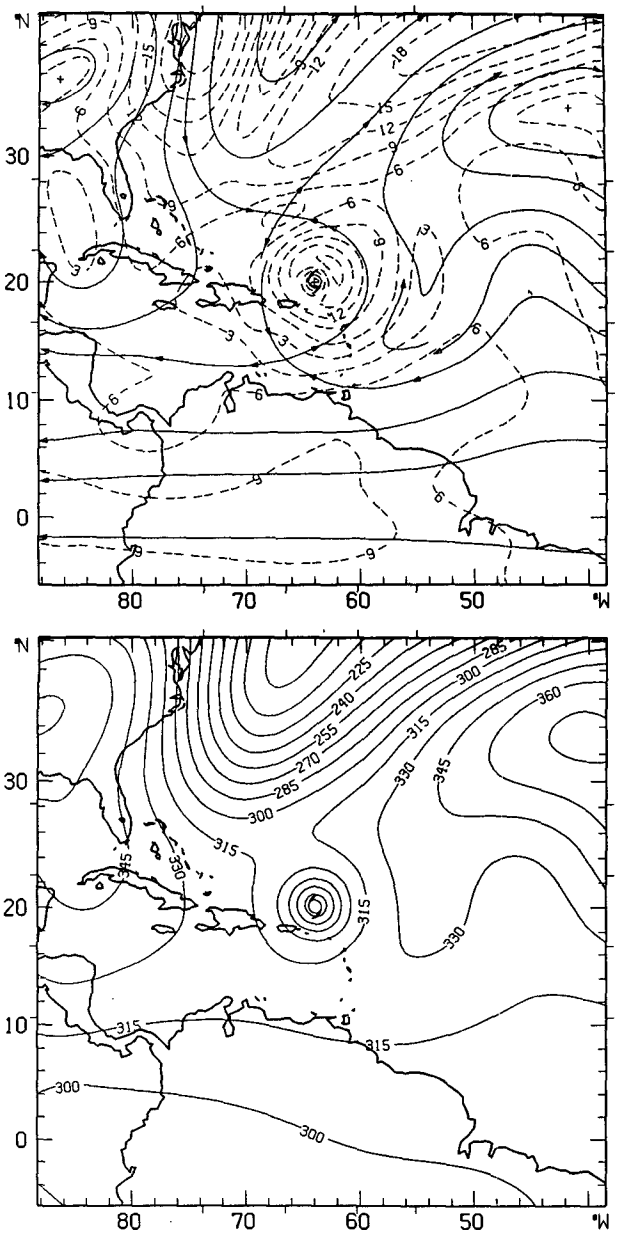

FIG. 4. Initial streamline–isotach (top) and height-deviation (bottom) fields on meshes 1–3 of the prediction model for Hurricane Dean at 0000 UTC 4 August 1989. The streamlines are solid, the isotachs are dashed, and the deviation heights are from the balance equation. The isotach and height contour intervals are 3 m s^{-1} and 15 m, respectively.

4. Forecast results

a. 1989 Atlantic hurricane season

The VICBAR system was tested during the 1989 Atlantic hurricane season. The analyses were performed at four vertical levels (850, 700, 500, and 200 mb). Tests with smaller and larger numbers of levels indicated that four levels was the minimum number that could be used to adequately estimate the 850–200-mb average. The winds and heights on the synoptic-scale domain and the background field on the storm-environment domain were determined from the NMC regional analysis. Table 1 summarizes the mesh structure for the 1989 version of the prediction model. Although the outer domains extend well into the

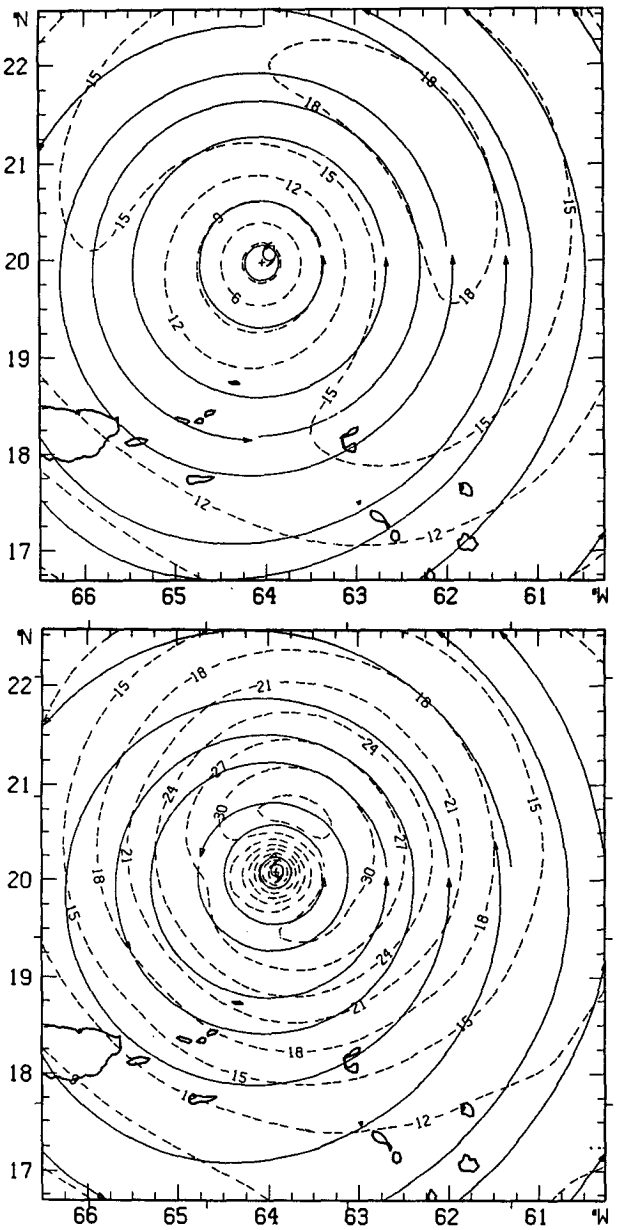

FIG. 5. The initial streamline–isotach fields in the operational (top) and high-resolution (bottom) versions of the model for Hurricane Dean at 0000 UTC 4 August 1989.

Southern Hemisphere, the regional analysis only extends to the equator. For this reason, u and h in the Southern Hemisphere were determined by assuming symmetry across the equator, and v was determined by assuming antisymmetry. In the 1989 version of the model, the lateral boundary condition defined by (3.6) was used. Because this condition essentially holds the fields fixed at the boundaries, the outer domain was made very large to minimize the boundary effects on the interior meshes.

The input for VICBAR (the observations and NMC regional analyses) for the 0000 and 1200 UTC forecasts were collected in real time. The VICBAR system was adapted to the operational environment during the 1989 season. All of the forecasts were rerun at the end of the season with the final version of the forecasting system. Thus, the results presented here were not run in real time. However, no changes were made to the operational data files, and operational initial positions, initial storm-motion vectors, and vortex parameters were used in all of the forecasts performed at the end of the season.

VICBAR was run for nearly all of the synoptic times for which a named tropical cyclone was present in the Atlantic basin. The track forecasts were verified by comparison with the NHC "best track," the track of the storm center determined by a poststorm analysis of all available observations. The forecast error is defined as the great circle distance between the forecast position and the best-track position. The forecasts were verified only for cases of tropical-storm strength or greater.

VICBAR is compared with other track guidance models that are available to the forecasters at NHC. The simplest guidance model is CLIPER (climate and persistence), which uses climatological and persistence factors to predict storm tracks. The CLIPER model is used as a baseline for determining the skill of other models. Forecast errors are presented in terms of a relative error RE defined by

$$\mathrm{RE} = \frac{100(\mathrm{ME} - \mathrm{CE})}{\mathrm{CE}}, \qquad (4.1)$$

where ME is the average model error and CE is the

TABLE 1. The mesh structure for the prediction model used in 1989.

Mesh	Nodal spacing (km)	X-domain length (km)	Y-domain length (km)	Latitude boundaries	Longitude boundaries	Time step (s)
1	50	600	600	Variable	Variable	75
2	100	1800	1800	Variable	Variable	150
3	200	4800	4800	Variable	Variable	300
4	400	14 400	11 200	26°–66°N	155°–5°W	600
5	800	19 200	16 000	46°–75°N	180°–20°E	1200

average CLIPER error for the same forecast cases. A negative value of RE indicates forecast skill.

The other track models in the forecast comparison include a 1) statistical–dynamical model (NHC83) that combines CLIPER-type input and geopotential heights from NMC's aviation model to produce a statistical track forecast; 2) three-dimensional mesoscale model designed specifically for hurricane forecasting (QLM, quasi-Lagrangian model); 3) model that follows a trajectory in the aviation model with a correction that accounts for the beta effect (BAM, beta and advection model); and 4) barotropic track-forecast model (SANBAR, Sanders barotropic model). The primary differences between VICBAR and SANBAR are that VICBAR has a larger horizontal domain, greater horizontal resolution in the vicinity of the vortex, and a more sophisticated objective analysis scheme. These operational track forecast models are described in more detail by DeMaria et al. (1990). The statistical–dynamical model NHC83 had the smallest mean forecast errors relative to the other operational models during 1983–1988. However, the predecessor to QLM (MFM, moveable fine-mesh model; Hovermale and Livezey 1977) was used, and BAM was not available from 1983 to 1988.

Figure 6 shows comparisons of VICBAR with each of the operational track prediction models in terms of relative error. VICBAR was compared with each model separately to maximize the homogeneous sample size, because not all of the operational models were available at each forecast time. VICBAR had skill for all forecast periods out to 72 h as indicated by the negative values of RE. In general, VICBAR had greater skill than QLM, BAM, and SANBAR, and skill comparable with NHC83.

A paired t test (e.g., Larsen and Marx 1981) was used to determine the statistical significance of the difference between the mean forecast errors from different models. For example, to determine whether the mean errors for VICBAR were significantly smaller than those from CLIPER, the difference between the forecast error from each model was calculated for each forecast in the sample. The null hypothesis was that the mean of the differences was not significantly different from zero. The familiar t statistic and (two-sided) distribution were used for the significance testing. The 95% confidence level was used to determine whether the mean errors between two models were significantly different.

Most of the forecasts are separated by 12 h. Neumann et al. (1977) has indicated that forecasts separated by less than ~30 h may not be independent. To account for this, an effective sample size, N^*, is estimated for each verification time using this 30-h criterion. If the time interval between two forecasts (Δt) is <30 h, the second forecast is counted as a fractional case ($\Delta t/30$). Following Laurmann and Gates (1977),

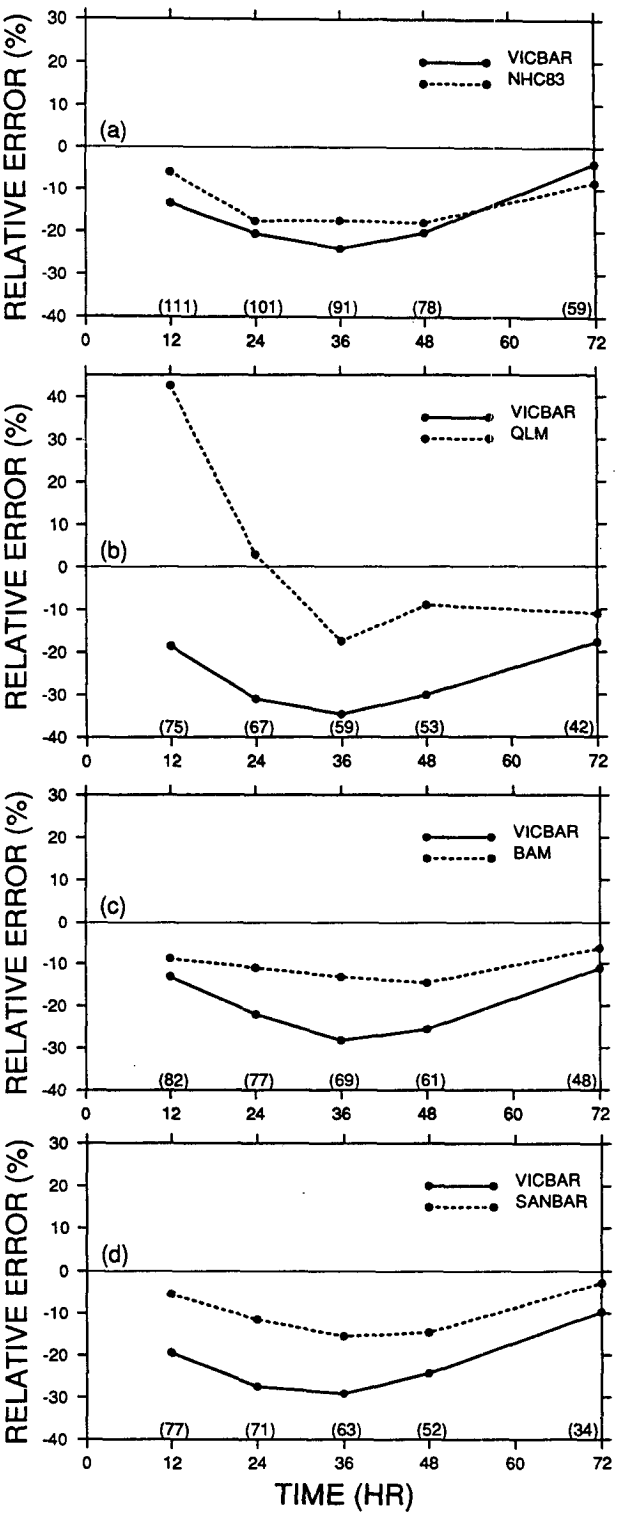

FIG. 6. Average relative errors from VICBAR and (a) NHC83, (b) QLM, (c) BAM, and (d) SANBAR for 1989. The average errors from VICBAR and each of the other models (including CLIPER used for the calculation of relative error) are from homogeneous samples. The number of cases at each forecast time is indicated along the bottom of each diagram.

TABLE 2. Results from the paired t test for the 1989 model track-error comparisons. VICBAR and CLIPER are compared with each of the other models for homogeneous samples, The Y (N) indicates that the average forecast error difference was significant (not significant) at the 95% level. Results are shown for the 12-, 24-, 36-, 48-, and 72-h forecasts.

	VICBAR	QLM	VICBAR	NHC83	VICBAR	BAM	VICBAR	SANBAR
CLIPER	YYYYN	YNNNN	NYYNN	YYYYN	NYYYN	NNNNN	YYYYN	NNNNN
VICBAR		YYNNN		NNNNN		NNNNN		YYYNN

the effective sample size N^* is then used in place of the true sample size N in the calculation of the t statistic and the degrees of freedom. The true sample size at each verification time is shown at the bottom of Figs. 6a–d. To a good approximation, the effective sample sizes are a factor of 2 less than the true sample sizes.

Table 2 shows the results of the significance testing for the forecast errors shown in Fig. 6. The significance testing was performed individually for homogeneous samples that included CLIPER, VICBAR, and each of the other models. The skill of VICBAR was significant at 12, 24, 36, and 48 h, as indicated by the comparison with CLIPER for the QLM and SANBAR samples. NHC83 was the only other model with significant skill during the 1989 season. The differences between VICBAR and QLM at 12 and 24 h, and between VICBAR and SANBAR at 12, 24, and 36 h, were also significant.

The results shown in Fig. 6a include some cases from every named tropical cyclone during the 1989 season. There was considerable variation of the performance of VICBAR (and the operational models) between individual storms. Part of the variability in the VICBAR track errors can be explained by the validity of the barotropic assumption in each forecast. Intense tropical cyclones might be expected to have stronger vertical coupling than weaker storms because of the convective activity and would, therefore, be better represented by a barotropic prediction model. Figure 7 shows that

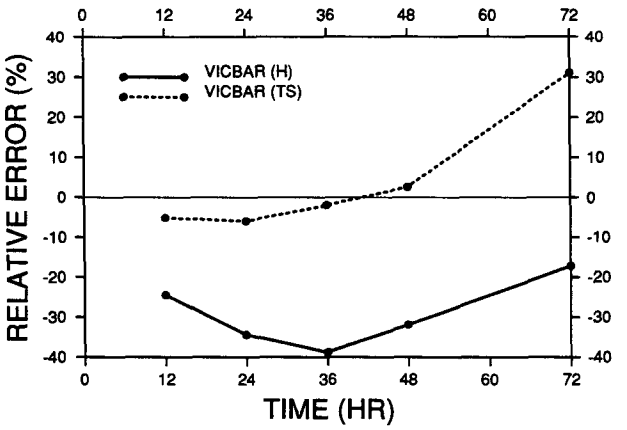

FIG. 7. Average relative errors from VICBAR for cases that were initially of tropical-storm intensity and for cases that were initially of hurricane intensity for 1989.

VICBAR had considerably greater skill for the more intense cases. The skill at 12, 24, 36, and 48 h was statistically significant for the hurricane cases, but was not significant at any forecast time for the tropical-storm cases. Most of the difference in the skill between the hurricane and tropical-storm cases in Fig. 7 was due to differences in VICBAR forecasts rather than to differences in the CLIPER forecasts (except at 72 h). For example, at 24, 48, and 72 h, the average errors for the VICBAR hurricane forecasts were 118, 281, and 511 km compared with 212, 381, and 599 km for the VICBAR tropical-storm cases. The average CLIPER error at 24, 48, and 72 h were 180, 412, and 617 km for the hurricane cases and 225, 373, and 457 km for the tropical-storm cases.

b. 1990 Atlantic hurricane season

A number of changes were made to VICBAR for the 1990 hurricane season. In order to extend the analysis into the Southern Hemisphere, the regional analysis background field was replaced with a 12-h forecast from the 0000 UTC medium-range forecast (MRF) or the 1200 UTC aviation global forecast models. The MRF model is run once per day and produces a 240-h forecast, and the aviation model produces a 72-h forecast twice per day. The MRF was used when available because it has a later data cutoff time than the aviation run. A 12-h forecast from the global model was used so that VICBAR could be run before the current global model forecast was completed. The winds and heights on the 2.5° lat–long grid on the synoptic-scale domain were obtained from an R40 truncation of the T80 global model forecasts (only the R40 files were available at NMC). Another change to the VICBAR analysis procedure was that a new vertical level (400 mb) was added to the synoptic-scale and storm-environment analyses.

Tropical cyclones usually exist in environments with low vertical wind shear. This may be one reason that skillful track forecasts can be made with a barotropic model. However, the tracks of tropical cyclones are often influenced by midlatitude troughs where baroclinic processes are important. To improve the VICBAR forecasts of the synoptic-scale environment, time-dependent boundary conditions were applied using vertically averaged winds and heights from the MRF or aviation models. Thus, $\bar{u}$, $\bar{v}$, and $\bar{h}$ in (3.1)–(3.3)

TABLE 3. The mesh structure for the prediction model used in 1990.

Mesh	Nodal spacing (km)	X-domain length (km)	Y-domain length (km)	Latitude boundaries	Longitude boundaries	Time step (s)
1	50	600	600	Variable	Variable	100
2	100	1800	1800	Variable	Variable	200
3	200	4800	4800	Variable	Variable	400
4	400	14 400	11 200	26°S–66°N	140°W–10°E	800

were obtained from the global model forecasts. These fields were obtained from the previous 12-h runs of the global models, similar to the procedure used to determine the background field. For the 0000 UTC VICBAR forecasts, $\bar{u}$, $\bar{v}$, and $\bar{h}$ are held fixed during the last 12 h of the 72-h forecast since these are not available from the previous 1200 UTC aviation run.

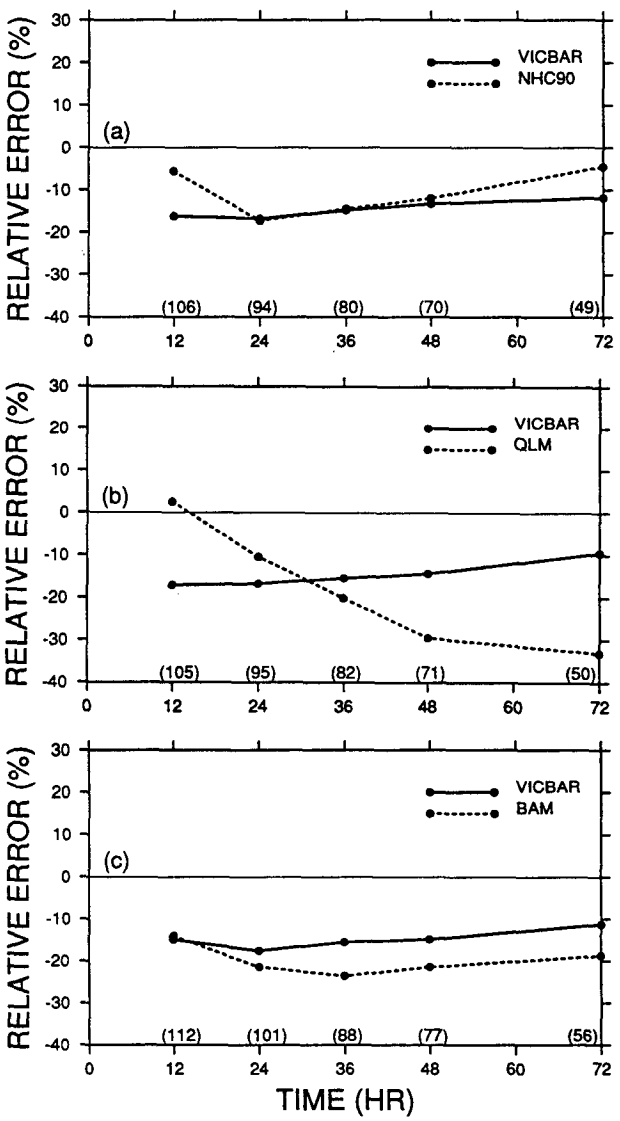

FIG. 8. Same as Fig. 6 for the 1990 VICBAR model.

The use of the time-dependent boundary conditions eliminated the need to constrain the amplitudes near the boundaries. Thus, the condition defined by (3.6) was no longer applied. The size of the model domain was also reduced, since the new boundary conditions were less restrictive than the condition defined by (3.6). Table 3 shows the mesh structure of the prediction model used in 1990. The resolution on the inner mesh was the same as the 1989 model (Table 1), but mesh 5 in the 1989 model was eliminated. The time step in the 1990 model was increased, since the outer domain does not extend as far north where the map factor becomes large.

The 1990 version of the model was usually available by ~5 h after the synoptic time for the 1200 UTC forecasts, while the 0000 UTC forecasts were usually run the following morning. All of the results presented for 1990 were run in real or near real time.

Figure 8 shows the average relative errors from VICBAR and each of the operational track-forecast models for 1990. SANBAR was not included in the comparison, since the 1990 SANBAR forecasts were not archived by NHC. Some minor revisions were made to NHC83 before the 1990 season, and its name was changed to NHC90. Figure 8 shows that VICBAR had skill at all forecast times between 12 and 72 h. The VICBAR skill was comparable with that of NHC90, but was less than that of QLM and BAM for the longer-range forecasts. A comparison of Figs. 6 and 8 shows that the skill of VICBAR and NHC90 was less in 1990 than in 1989, and QLM had considerably more skill in 1990 than in 1989. BAM also had more skill in 1990 than in 1989.

Table 4 shows the results of the significance tests for 1990. The skill of VICBAR (relative to CLIPER) was significant only at 12 h, and NHC90 had significant skill at 24 h. VICBAR and NHC83 had significant skill out to 48 h in 1989. QLM had significant skill at 48 and 72 h, and BAM had significant skill at 24 and 36 h. Neither BAM nor QLM had any significant skill in 1989.

The differences in the performance of the models in 1989 and 1990 may have been due to model changes

TABLE 4. Same as Table 2 for the 1990 model track-error comparisons.

	VICBAR	QLM	VICBAR	NHC90	VICBAR	BAM
CLIPER	YNNNN	NNNYY	YNNNN	NYNNN	NNNNN	NYYNN
VICBAR		YNNNN		NNNNN		NNNNN

and to differences in the types of storms in the two years. The improvement of QLM in 1990 may have been due to modifications that were made to refine the initialization in the vicinity of the storm (Mathur 1991). The decrease in the skill of VICBAR in 1990 may be related to the differences in the intensity of the storms in the two years. Figure 7 showed that, during 1989, VICBAR had considerably more skill for hurricanes than tropical storms, indicating that the VICBAR skill increases with the storm intensity. The storms in 1990 tended to be less intense than those in 1989, so a decrease in the skill of VICBAR might be expected.

The skill of VICBAR was also sensitive to the initial storm intensity during 1990 (except at 72 h), as shown in Fig. 9. However, the difference in skill between the hurricane and tropical-storm cases in 1990 was less than the difference in 1989. This disparity may be because the hurricanes in 1990 were less intense than in 1989.

c. *Evaluation of the VICBAR modifications for 1990*

Although some of the difference between the VICBAR skill in 1989 and 1990 may have been due to differences in the types of forecasts, some may have been due to the model modifications made for the 1990 season. For 31 cases (four storms) in 1989, additional data (boundary-condition fields and data for the 400-mb analyses) were collected for a separate study of the effect of satellite observations on the VICBAR forecasts.

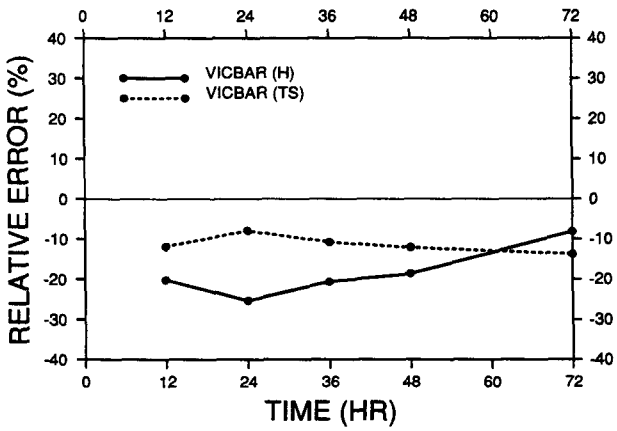

FIG. 9. Same as Fig. 7 for the 1990 VICBAR model.

This extra data allowed the 1990 version of the model to be used on the 1989 forecasts. In addition, data (background fields over the 1989 model domain) for 10 randomly selected cases (one for each storm with a 72-h verification) were obtained from history tapes at NMC to allow the 1989 version of the model to be run on the 1990 storms. These 41 cases could then be run with either version of the model.

The 1990 model includes 400-mb analyses, Southern Hemisphere data, time-dependent boundary conditions, and a background field from a 12-h-old global model forecast rather than the current regional analysis. Preliminary tests showed that the inclusion of the 400-mb level and the Southern Hemisphere data resulted in only small changes in the predicted storm track. The replacement of the regional analysis with a 12-h forecast and the inclusion of time-dependent boundary conditions had larger effects on the predicted storm tracks. To investigate the latter two effects, five versions of the model were tested. These included the 1990 operational version with a 12-h forecast background field and boundary conditions from a 12-h-old forecast (A12B12) and the 1989 operational version with a current background field and no time-dependent boundary conditions (A00Bxx). The model was also run with a 12-h forecast background field and boundary conditions from a current forecast (A12B00), with a current background field and boundary conditions from a 12-h-old forecast (A00B12), and with a current background field and boundary conditions from a current forecast (A00B00). It is unlikely that the A12B00 version would ever be used operationally since if the current boundary conditions were available, the current analysis would also be available. However, this version is useful for isolating the effect of using current versus 12-h-old fields.

Figure 10 shows that the 1989 version of the model (A00Bxx) had greater skill than the 1990 version (A12B12), except at 72 h for the homogeneous sample. This difference suggests that the use of a 12-h forecast background field degraded the VICBAR skill relative to using a current background field. This effect can also be seen by comparing A00B00 with A12B00 and by comparing A00B12 with A12B12. When the current background field was used in the 1990 version of the model (A00B12), the skill was about the same as the 1989 version of the model (A00Bxx).

Figure 10 also shows that the skill of the forecasts was sensitive to the quality of fields used on the bound-

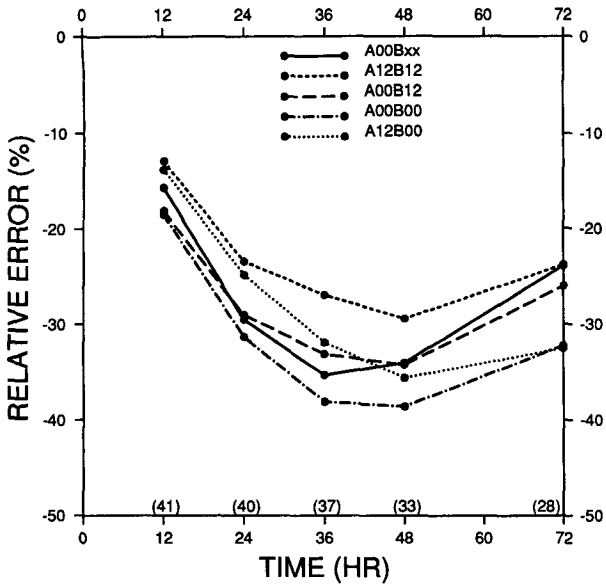

FIG. 10. Average relative errors for five versions of VICBAR for a homogeneous sample. The versions include A00Bxx (1989 operational), A12B12 (1990 operational), A00B12 (current regional analysis background field, 12-h-old boundary-condition fields), A00B00 (current regional background field, current boundary-condition fields), and A12B00 (12-h forecast background field, current boundary-condition fields).

aries. When the boundary fields were obtained from a current forecast rather than a 12-h-old forecast, the skill improved for the case when a 12-h forecast background field was used (compare A12B12 with A12B00) and for the case when a current background field was used (compare A00B12 with A00B00). This sensitivity of the model skill to the quality of the fields used on the boundaries is consistent with the case study presented by Kurihara et al. (1990).

The difference between the 1990 model skill (A12B12) and the skill of the model using a current background field and boundary conditions from the current global forecast (A00B00) in Fig. 10 was statistically significant at the 95% level at all forecast times after 24 h. However, the global-model forecast is usually unavailable until ~5 h after the synoptic time, so the VICBAR forecast would be unavailable until ~7 h after the synoptic time if the current global-model fields are used. When the background field and boundary conditions are obtained from a 12-h-old global forecast, as in the 1990 model, the VICBAR forecasts are available by 5 h after the synoptic time. The NHC advisories are normally issued four times per day (4 and 10 h after 1200 UTC and 2.5 and 10 h after 0000 UTC). If the VICBAR forecasts are available at 7 h after the synoptic time, they would still be useful for the advisories issued at 10 h after the synoptic time. Therefore, the A00B00 version of VICBAR will be used during the 1991 season.

d. Extended-range predictions

During 1990, the boundary conditions for the 1200 UTC VICBAR forecasts were obtained from the previous 0000 UTC MRF model, which is run to 240 h. This allowed VICBAR forecasts to be run for more than 72 h. To test the feasibility of extended-range prediction of tropical cyclones, all of the 1200 UTC forecasts were run to 120 h. Ten of these forecasts had 120-h verifications (six for Hurricane Isidore and four for Hurricane Gustav). Table 5 shows that the cases with the 120-h verifications had much smaller forecast errors than the total 1990 sample and considerably greater skill. For example, at 72 h the relative error defined by (4.1) is −54% for the 10-case sample, compared with −12% for the total 1990 sample. This result probably occurred because Isidore and Gustav were the two most intense storms of the 1990 season, and VICBAR has greater skill for more intense systems. It is difficult to determine the skill of the 96- and 120-h forecasts, since no other models provide 5-day track forecasts. However, Table 5 demonstrates that extended-range predictions are feasible when the synoptic-scale forecasts from a global model are used (in this case as boundary conditions).

5. Concluding remarks

A numerical method for including a wide range of horizontal scales of motion was applied to a barotropic forecast model. The numerical method uses cubic B-spline representations of variables on nested domains, and is referred to as the SAFER (spectral application of finite-element representation) method. The SAFER method was used for the objective analysis of observations and the solution of the prediction equations (shallow-water equations on a Mercator projection). This analysis and forecasting system is referred to as VICBAR.

The VICBAR model was tested on data collected in real time during the 1989 Atlantic hurricane season and was run operationally during the 1990 season. For the 1989 season, VICBAR had skill that was comparable with or greater than that of the operational track-

TABLE 5. VICBAR and CLIPER average forecast errors (km) for the ten cases with 120-h verification and for the total 1990 sample.

	Forecast error (km)			
	120-h cases		Total 1990 sample	
t (h)	VICBAR	CLIPER	VICBAR	CLIPER
24	105	171	178	213
48	194	434	383	442
72	333	723	581	659
96	565	—	—	—
120	775	—	—	—

forecast models. For the 1990 season the skill was comparable with that of the operational models. In both 1989 and 1990, VICBAR had considerably more skill for forecasts of hurricanes than for forecasts of tropical storms (except at 72 h in 1990).

For the 1990 season, VICBAR was generalized to include time-dependent boundary conditions from a global forecast model. These boundary conditions improved the VICBAR forecasts, especially at the longer ranges (60–72 h). When the boundary conditions were obtained from the MRF model (which is run for 240 h), 5-day VICBAR track forecasts were produced. The skill of VICBAR is sensitive to the choice of the background field used in the objective analysis and the boundary condition fields. The use of a background field and boundary-condition fields from a 12-h-old global-model forecast (appropriately lagged) significantly reduces the VICBAR skill relative to the use of fields from the current global forecast.

The skill of VICBAR suggests that the motion of tropical cyclones can be predicted with a barotropic model (especially for intense systems). However, the prediction of the surrounding synoptic-scale flow clearly requires the inclusion of baroclinic and physical processes. A hybrid model similar to the 1990 version of VICBAR that predicts the motion of the storm using barotropic physics, but that also includes boundary information from a more general model, may be a useful tool for accurately forecasting tropical cyclone motion on relatively small computing systems. All that would be necessary is access to a global model forecast and enough computer resources to integrate a barotropic prediction model.

The success of VICBAR also demonstrates the usefulness of the SAFER method for the prediction of tropical cyclones using initial conditions from observations, although additional interior meshes would probably be required when vertical structure and physical processes are included. The SAFER method has also been applied to a barotropic model (Shapiro and Ooyama 1990) and a three-layer baroclinic model with simplified physical parameterizations (Shapiro 1992) to study tropical cyclone motion based upon idealized initial conditions. Development of a fully three-dimensional model that uses the SAFER method is currently under way.

Acknowledgments. The authors thank James Franklin and Lloyd Shapiro for their comments on this manuscript, and Robert Kohler for his help with the data collection. The manuscript was prepared by Gail Derr.

REFERENCES

Cressman, G. P., 1958: Barotropic divergence and very long atmospheric waves. *Mon. Wea. Rev.*, **86**, 293–297.

DeMaria, M., 1985: Tropical cyclone motion in a nondivergent barotropic model. *Mon. Wea. Rev.*, **113**, 1199–1210.

——, M. B. Lawrence, and J. T. Kroll, 1990: An error analysis of Atlantic tropical cyclone track guidance models. *Wea. Forecasting*, **5**, 47–61.

Frank, W. M., 1977: The structure and energetics of the tropical cyclone I. Storm structure. *Mon. Wea. Rev.*, **105**, 1119–1135.

Fulton, S. R., and W. H. Schubert, 1987: Chebyshev spectral methods for limited area models. Part I: Model problem analysis. *Mon. Wea. Rev.*, **115**, 1940–1953.

Hovermale, J. B., and R. E. Livezey, 1977: Three-year performance characteristics of the NMC hurricane model. Preprints, *11th Tech. Conf. Hurricanes and Tropical Meteorology*, Miami, Amer. Meteor. Soc., 122–124.

Kurihara, Y., M. A. Bender, R. E. Tuleya, and R. J. Ross, 1990: Prediction experiments of Hurricane Gloria, 1985, using a multiply nested movable mesh model. *Mon. Wea. Rev.*, **118**, 2185–2198.

Larsen, R. J., and M. L. Marx, 1981: *An Introduction to Mathematical Statistics and Its Applications.* Prentice-Hall, Inc., 530 pp.

Laurmann, J. A., and W. L. Gates, 1977: Statistical considerations in the evaluation of climatic experiments with atmospheric general circulation models. *J. Atmos. Sci.*, **34**, 1187–1199.

Leith, C. E., 1974: Spectral statistical-dynamical forecast experiments. *Report, Inter. Symp. on Spectral Methods in Numerical Weather Prediction,* Working Group on Numerical Experiments, Global Atmospheric Research Program.

Lord, S. J., and J. L. Franklin, 1987: The environment of Hurricane Debby (1982). Part I: Winds. *Mon. Wea. Rev.*, **115**, 2760–2780.

Mathur, M. B., 1991: The National Meteorological Center's quasi-Lagrangian model for hurricane prediction. *Mon. Wea. Rev.*, **119**, 1419–1447.

Merrill, R. T., 1984: A comparison of large and small tropical cyclones. *Mon. Wea. Rev.*, **112**, 1408–1418.

Neumann, C. J., M. B. Lawrence, and E. L. Caso, 1977: Monte Carlo significance testing as applied to statistical tropical cyclone prediction models. *J. Appl. Meteor.*, **16**, 1165–1174.

Ooyama, K. V., 1984: A model for hurricane prediction. Postprints, *15th Conf. on Hurricanes and Tropical Meteorology,* Miami, Amer. Meteor. Soc., 344–349.

——, 1987: Scale-controlled objective analysis. *Mon. Wea. Rev.*, **115**, 2479–2506.

Shapiro, L. J., 1992: Hurricane vortex motion and evolution in a three-layer model. *J. Atmos. Sci.*, **49**, 140–153.

——, and K. V. Ooyama, 1990: Barotropic vortex evolution on a beta plane. *J. Atmos. Sci.*, **47**, 170–187.

Willoughby, H. E., J. A. Clos, and M. G. Shoreibah, 1982: Concentric eyewalls, secondary wind maxima, and the evolution of the hurricane vortex. *J. Atmos. Sci.*, **39**, 395–411.